Ⅲ．研究成果の刊行に関する一覧表

書　籍

著者名	論文タイトル名	書籍全体の編集者名	書　籍　名	出版社名	出版地	出版年	ページ
稲田有史，中村達雄，森本　茂，飯田秀之，古家　仁，諸井慶七郎	人工神経移植術を用いた末梢神経生体内再建法	光嶋　勲	PEPARS 末梢神経再建 － up date －	㈱全日本病院出版会	東京	2005	12～17
中村達雄，茂野啓示	確立した再生医療の基本コンセプト	茂野啓示	新・一から学ぶ歯周外科の手技	医歯薬出版	東京	2005	356～361
稲田有史，中村達雄	末梢神経損傷に対する生体内再生治療 －Polyglycolic Acid-Collagen Tube による CRPS Type II の外科的治療－	小川節郎	痛み治療のアプローチ	真興交易㈱医書出版部	東京	2005	94～112
金丸眞一，伊藤壽一	小耳症における先天性外耳道閉鎖症と聴力の問題点	福田　修，荻野洋一	耳介の形成外科	克誠堂出版	東京	2005	25～35

雑　誌

発表者氏名	論文タイトル名	発表誌名	巻号	ページ	出版年
Omori K, Nakamura T, Kanemaru S, Asato R, Yamashita M, Tanaka S, Magrufov A, Ito J, Shimizu Y	Regenerative medicine of the trachea: The first human case	Ann Otol Rhinol Laryngol	114(6)	429～433	2005
Yokoyama S, Kano M, Watanabe M, Ogawa H, Omori K	Morphological and histologic examination of the epiglottis: Implications for improving epiglottic closure technique	Ann Otol Rhinol Laryngol	115(1)	23～29	2006
Liu K, Kozono D, Kato Y, Agre P, Hazama A, Yasui M.	Conversion of aquaporin 6 from an anion channel to a water-selective channel by asingle amino acid substitution	Proc NatlAcad Sci	102(6)	2192～2197	2005
Morino S, Nakamura T, Toba T, Takahashi M, Kushibiki T, Tabata Y, Simizu Y	Fibroblast growth factor-2 indues recovery of pulmonary blood flow in canine emphysema models	Laboratory and Animal Investigations	128	920～926	2005
Inada Y, Morimoto S, Moroi K, Endo K, Nakamura T	Surgical relief of causalgia with an artificial nerve guide tube: Successful surgical treatment of causalgia (Complex Regional Pain Syndrome Type II) by in situ tissue engineering with a polyglycolic acid-collagen tube	Pain	117	251～258	2005
Lynn AK, Nakamura T, Patel N, Porter AE, Renouf AC, Laity PR, Best SM, Cameron RE, Shimizu Y, Bonfield W	Composition-controlled nanocomposites of apatite and collagen incorporating silicon as an osseopromotive agent	J Biomed Mater Res	74A	447～453	2005

発表者氏名	論文タイトル名	発表誌名	巻号	ページ	出版年
Fukuda S, Nakamura T, Kishigami Y, Endo K, Azuma T, Fujikawa T, Tsutsumi S, Shimizu Y	New canine spinal cord injury model free from laminectomy	Brain Research Protocols	14	171～180	2005
Kanemaru S, Nakamura T, Omori K, Magrufov A, Yamashita M, Ito J	Regeneration of mastoid air cells in clinical applications by in situ tissue engineering	Laryngoscope	115(2)	253～258	2005
Kanemaru S, Nakamura T, Yamashita M, Magrufov A, Kita T, Tamaki H, Tamura Y, Iguchi F, Kim TS, Kishimoto M, Omori K, Ito J	Destiny of autologous bone marrow-derived stromal cells implanted in the vocal fold	Ann Otol Rhinol Laryngol	114(12)	907～912	2005
大森孝一，中村達雄，金丸眞一，安里　亮，山下 勝，清水慶彦	〔肺病変の修復・再生へのアプローチ〕組織工学からみた臓器再生 －気管・気管支の再生治療－	日本臨床麻酔学会誌	25(3)	310～315	2005
大森孝一	再生医療の現状と今後の展開	平成17年度福島県国保地域医療学会	抄録集	83～101	2006
多田靖宏，野本幸男，鈴木輝久，大森孝一	気道の再生	喉頭	17(2)	84～88	2005
中村達雄	＜特集 肺の再生医療～現状と展望＞ 気道の再生	呼吸と循環	53(2)	119～125	2005
野田澤俊介，中村達雄，清水慶彦，瀧川敏算	メッシュ型人工気管の力学特性	材料	54(1)	85～89	2005
高橋　充，加藤治文，中村達雄，清水慶彦	＜特集 肺の再生医療～現状と展望＞ EPC による肺高血圧の治療	呼吸と循環	53(2)	159～165	2005
中原　貴，中村達雄，小林英三郎，呉本晃一，松野智宣，田畑泰彦，江藤一洋，清水慶彦	歯根膜由来細胞播種による歯周組織の In situ ティッシュ・エンジニアリング	歯科臨床研究	2	28～34	2005
金丸眞一	頭頸部領域の再生医療	日本耳鼻咽喉科学会会報	108(4)	330～331	2005
金丸眞一	難治性中耳炎に対する再生医学アプローチ　－in situ tissue engineering による乳突蜂巣再生の試み－	Otology Japan	15	195～202	2005
金丸眞一	頭頸部領域の再生医療	頭頸部癌	31(3)	402～407	2005
金丸眞一	人工神経チューブによる神経再生医療	喉頭	17(2)	84～88	2005
金丸眞一	＜トピックス＞頭頸部領域の再生医療	日本耳鼻咽喉科学会専門医通信	85号	28～29	2005

Ⅳ. 研究成果の刊行物・別刷

Annals of Otology, Rhinology & Laryngology 114(6):429-433.

Regenerative Medicine of the Trachea: The First Human Case

Koichi Omori, MD; Tatsuo Nakamura, MD; Shinichi Kanemaru, MD; Ryo Asato, MD; Masaru Yamashita, MD; Shinzo Tanaka, MD; Akhmar Magrufov, MD; Juichi Ito, MD; Yasuhiko Shimizu, MD

Objectives: The objective of the present study was to demonstrate regenerative medicine of the tracheal tissue by using an in situ tissue engineering technique for airway reconstruction.

Methods: Based on the previous successful experimental animal studies, the current regenerative technique was applied to repair of the trachea of a 78-year-old woman with thyroid cancer. A Marlex mesh tube covered by collagen sponge was used as a tissue scaffold. The operative intervention included right hemithyroidectomy, resection of the trachea, and tracheoplasty using the scaffold. The right half of three rings of the trachea was resected, and the scaffold material was sutured to the defect of the trachea.

Results: After 2 weeks, the mesh collagen structure of the artificial material could be seen with endoscopy in most of the implanted area. The artificial material was covered with epithelial growth after 2 months. Epithelialization continued to cover the artificial material completely for 2 years without any complications.

Conclusions: The current regenerative technique avoided tracheotomy, a second operation, and deformity. Good epithelialization has been observed on the tracheal luminal surface without any complications for 2 years. Although long-term observation is required, regenerative medicine of the tracheal tissue appears feasible for airway reconstruction.

Key Words: airway reconstruction, in situ tissue engineering, regenerative medicine, trachea.

INTRODUCTION

Airway reconstruction after resection of malignancies or stenotic inflammatory lesions is one of the most difficult treatments. Ideally, both the airway framework and the endotracheal surface should be reconstructed. Cartilage grafts, muscle grafts, bone grafts, and skin grafts have been placed in the defect after resection of lesions of the trachea.[1,2] These techniques require several complicated procedures. Postoperative airway stenosis sometimes occurs because of scar, granulation tissue, and submucosal fibrosis.

Various types of artificial trachea have been used; however, almost all of these trials have ended unsuccessfully.[3] Our group has developed a porous type of artificial trachea coated with collagen sponge designed to induce tissue invasion into the Marlex mesh scaffold, thus assisting reepithelialization of the lumen and helping to avoid the formation of granulation tissue and dehiscence at the interface between the prosthesis and the host tissue.[4-7]

Recently, progress in tissue engineering has made it possible to fabricate some tissues or organs such as skin, bone, cartilage, and muscle.[8] Tissue engi-

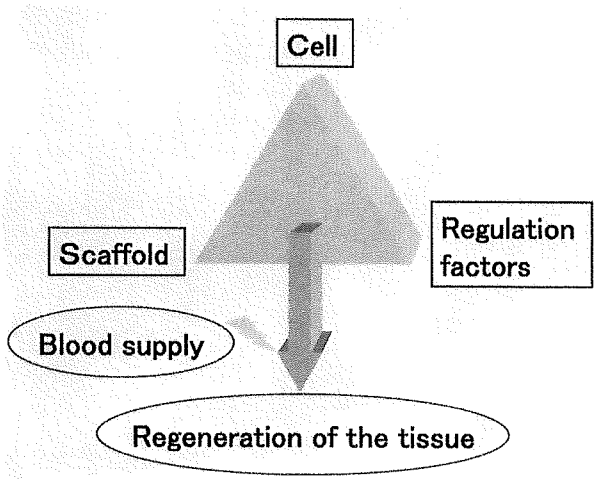

Fig 1. Three factors necessary for tissue regeneration.

From the Department of Otolaryngology, Fukushima Medical University, School of Medicine, Fukushima City (Omori); and the Department of Bioartificial Organs, Institute for Frontier Medical Sciences (Nakamura, Shimizu), and the Department of Otolaryngology–Head and Neck Surgery, Postgraduate School of Medicine (Omori, Kanemaru, Asato, Yamashita, Tanaka, Magrufov, Ito), Kyoto University, Kyoto; Japan. This study was supported in part by a Grant-in-Aid for Scientific Research (B) from the Japan Society for the Promotion of Science and in part by a grant of Health and Labor Science Research Grants for Research on Human Genome, Tissue Engineering, from the Ministry of Health, Labor and Welfare.

Presented at the meeting of the American Laryngological Association, Phoenix, Arizona, April 30–May 1, 2004.

Correspondence: Koichi Omori, MD, Dept of Otolaryngology, Fukushima Medical University, 1 Hikarigaoka, Fukushima City, 960-1295, Japan.

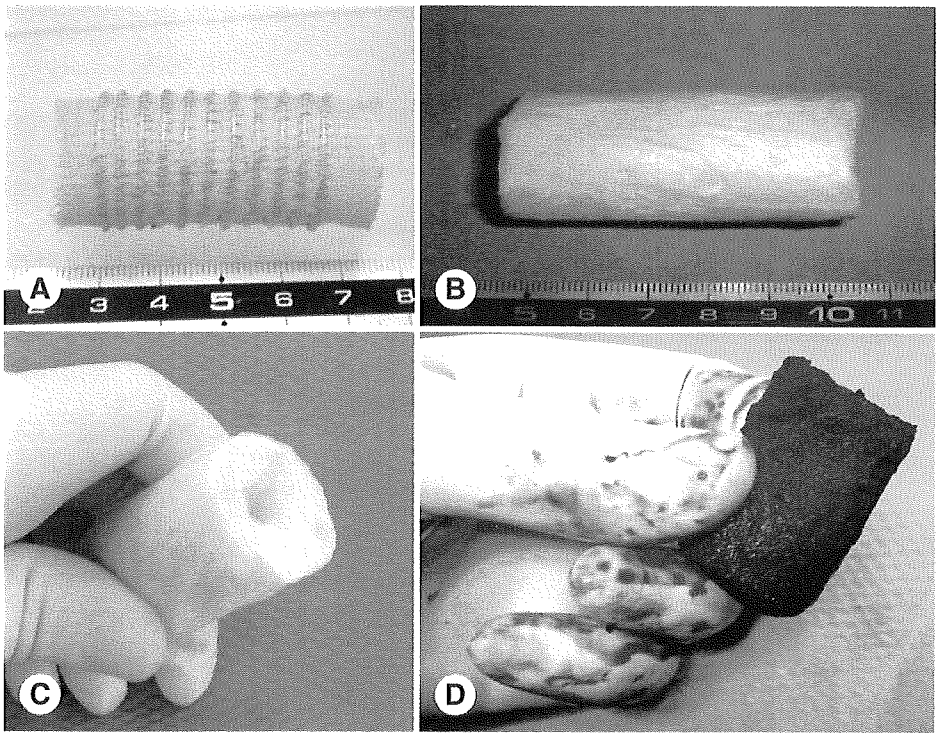

Fig 2. Artificial material. **A)** Marlex mesh tube with spiral ring. **B)** Marlex mesh tube with spiral ring coated with collagen sponge. **C)** Artificial material trimmed to size of defect. **D)** Injection of autologous blood into collagen sponge.

neering technology consists of three factors: scaffold, cells, and regulation factors, as shown in Fig 1. Depending on the situation at the site of application, these elements are chosen and applied in combination. On the basis of the novel concept of in situ tissue engineering, in contrast to ex vivo tissue engineering, our group has developed a collagen sponge scaffold to support tissue regeneration and has used it successfully to repair defects in the trachea, esophagus, stomach, and intestine in animal models.[4-7,9-11] The collagen sponge scaffold provides favorable conditions for tissue regeneration in vivo in combination with infiltrated host cells and regulation factors released from the surrounding tissue.

Previously, for the experimental studies of an animal model for airway regeneration, 32 beagle dogs were used for operation under general anesthesia. The animal care, housing, and surgery followed the Guidelines of the Animal Experiment Committee, Kyoto University (1983).

In 24 of the 32 dogs, a 45-mm segment of the tra-

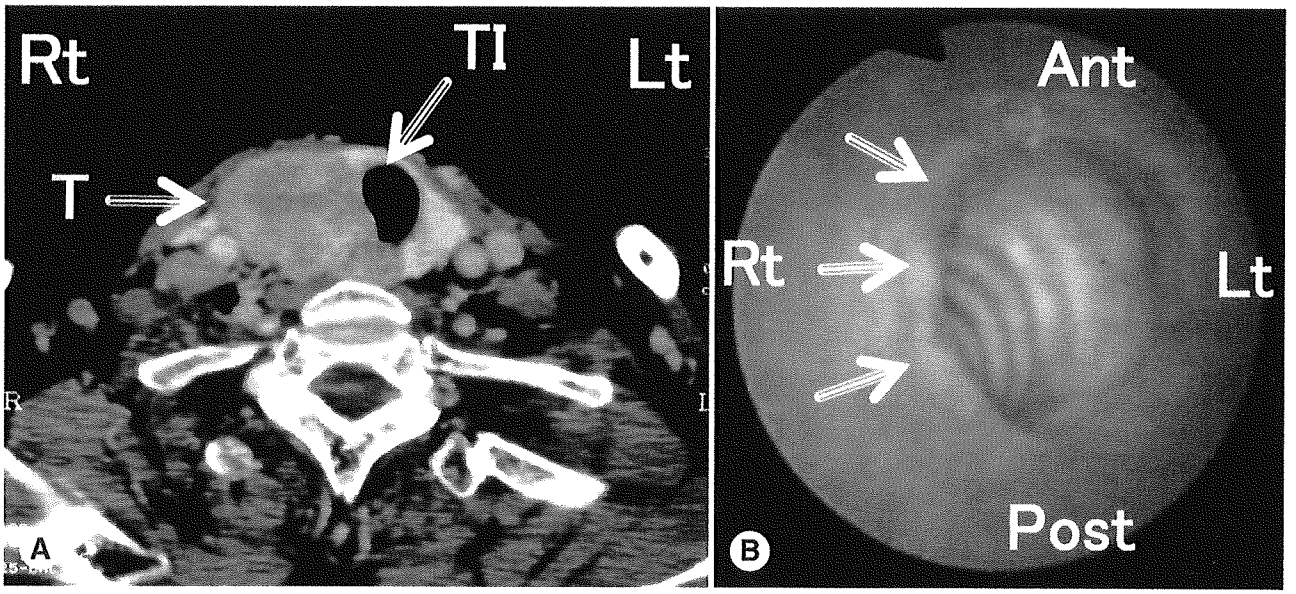

Fig 3. Preoperative investigation. **A)** Computed tomography scan. T — tumor, TI — tracheal invasion. **B)** Endoscopic findings. Arrows indicate tumor invasion into trachea.

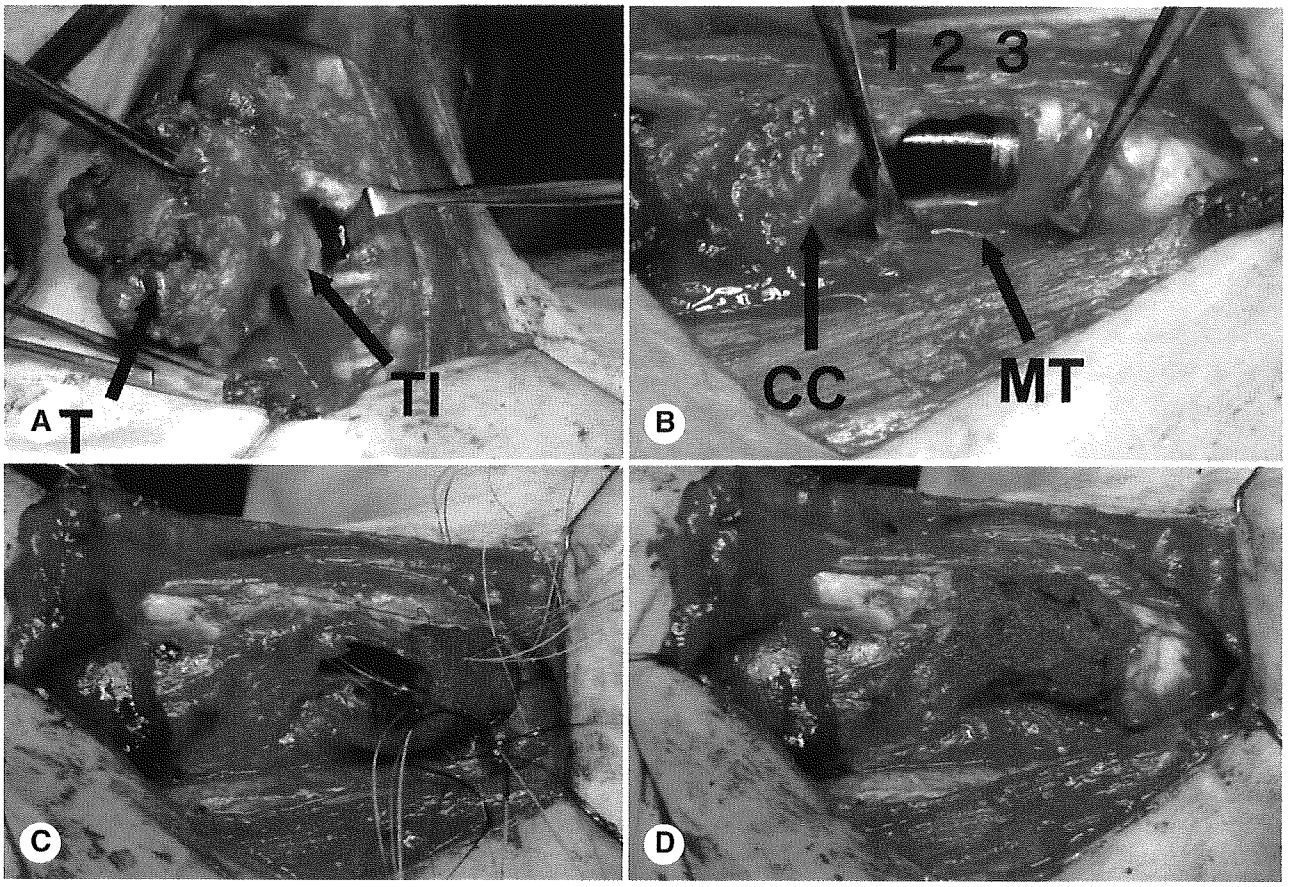

Fig 4. Operative procedures. **A)** Invasion of tracheal cartilage by tumor (T) of right lobe of thyroid gland. TI — tracheal invasion. **B)** Resected tracheal cartilage. CC — cricoid cartilage, MT — membranous trachea, 1 — first tracheal ring, 2 — second tracheal ring, 3 — third tracheal ring. **C)** Suturing of artificial material to defect. **D)** After implantation of artificial material.

chea was resected circumferentially 30 mm from the carina, and the Marlex mesh tube with collagen sponge was implanted as a scaffold material.[6] Postoperative endoscopy for a period of 3 to 60 months showed a well-epithelialized tracheal lumen without airway obstruction.[7] Light microscopy showed that the Marlex mesh was completely incorporated within the connective tissue. Scanning electron microscopy showed regeneration of the cilial epithelium. Mechanical tests showed that the stress-strain curve of the regenerated tissue was similar to that of the normal tracheal cartilage, demonstrating a firmly supported airway framework.

In 8 of the 32 dogs, the anterior part of the cricoid cartilage and/or the cartilaginous part of rings 1 through 5 of the trachea were resected. As a scaffold material, a Marlex mesh tube with collagen sponge was implanted into the defect. Postoperative endoscopy for a period of 3 to 26 months showed a well-epithelialized luminal surface with no airway stenosis in any of the 8 dogs. Although granulation was observed in 2 cases and a small part of the Marlex mesh was exposed in 1 case, these dogs were asymptomatic in terms of respiration.[12]

On the basis of the previous experimental studies of tracheal tissue regeneration using an in situ tissue engineering technique in animal models, this regenerative technique was applied for repair of the tracheal defect in a human case of tracheal invasion from thyroid cancer.

SCAFFOLD MATERIAL

An artificial material — a Marlex mesh tube covered by collagen sponge — was used for the tissue scaffold. An approximately 50-mm-long Marlex mesh tube with an outer diameter of 15 mm was made from polypropylene mesh with a pore size of 260 μm (CR Bard Inc, Billerica, Massachusetts) and implanted in a human case as presented below (Fig 2A). This tube was reinforced with a polypropylene spiral ring. The inner and outer sides of the Marlex mesh tube were coated with collagen sponge made from porcine dermal atelocollagen (Nippon Meatpackers Inc, Ibaraki, Japan) consisting of type 1 and type 3 collagen dissolved in hydrochloric acid solution, pH 3.0, at a concentration of 1.0% (Fig 2B). The artificial tube was corona-discharged at 9 kV to activate the polymer surface in order to immobilize the colla-

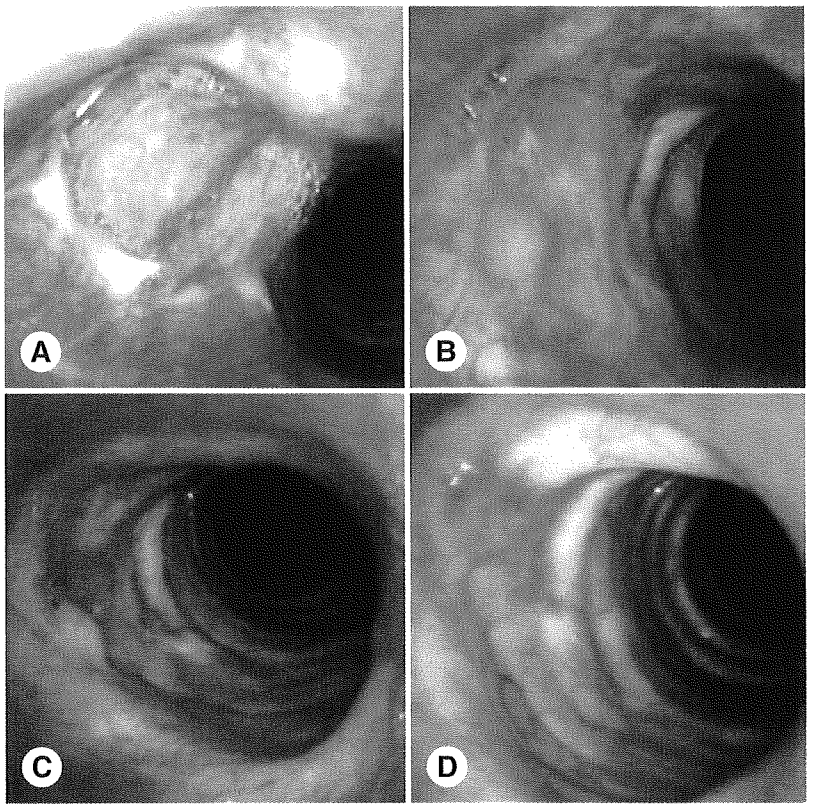

Fig 5. Endoscopic findings. **A)** After 2 weeks. **B)** After 2 months. **C)** After 7 months. **D)** After 20 months.

gen molecules and was heated at 140°C in vacuo in order to induce cross-linking between the collagen molecules.

CASE REPORT

This newly developed method for regeneration of the tracheal tissue was applied to a human patient for evaluation of its practical use in accordance with the guidelines of the Ethics Committee, Kyoto University Graduate School and Faculty of Medicine. A 78-year-old woman had swelling in the right side of her neck. A computed tomography scan showed heterogeneous tumor involving the right lobe of the thyroid gland, as shown in Fig 3A. Fine-needle aspiration biopsy of the tumor revealed papillary adenocarcinoma, class V. Preoperative testing showed a thyroid-stimulating hormone level of 8.9 μU/mL, a free tetraiodothyroxine level of 1.12 ng/dL, a free triiodothyroxine level of 3.74 pg/mL, and a thyroglobulin level of 423 ng/mL. Endoscopic examination showed bulging of the right luminal surface of the trachea, just below the subglottis (Fig 3B). This finding indicated tumor invasion into the tracheal tissue.

With informed consent, the patient underwent the current regenerative treatment of the tracheal tissue using the artificial material in 2002. Under general anesthesia, the operative intervention included right hemithyroidectomy, resection of the trachea, and tracheoplasty using the artificial material, Marlex mesh with collagen sponge. The artificial material was trimmed (Fig 2C), and autologous venous blood was injected into the collagen for air-tightness, watertightness, and release of endogenous factors (Fig 2D). The tumor had invaded the second ring of the tracheal cartilage on the right side (Fig 4A). The right half of three rings of the trachea was resected (Fig 4B). The material was sutured to the edge of the trachea with 4-0 Vicryl absorbable thread (Fig 4C,D). When the anesthesia had worn off, the endotracheal tube was removed in the operating room. After 2 weeks, the mesh collagen structure of the artificial material could be seen with endoscopy in most of the implanted area (Fig 5A). The artificial material was covered with epithelial growth after 2 months (Fig 5B). Good epithelialization was shown on most of the artificial material after 7 months (Fig 5C). Epithelial growth had covered the artificial material completely by 20 months with no complications (Fig 5D), and further observation approximately 5 months later supported this conclusion.

DISCUSSION

Reconstruction of the larynx and trachea in cases of malignancies or stenotic lesions is one of the most difficult surgical treatments. Bone graft, cartilage graft, muscle graft, and skin graft, among other techniques, have been used for repair of the airway defect.[1,2] These techniques following laryngeal and/or

tracheal resection required several complicated procedures for reconstructing both the airway framework and the luminal surface.

Artificial tracheal prostheses have been developed; however, almost all of the trials have ended unsuccessfully. Although the prosthesis of Neville et al,[3] which was made of silicone rubber with terminal Dacron suture rings, was once used clinically, dehiscence occurred at the interface between the prosthesis and the host tissue. Our group developed porous tracheal prostheses made of Marlex mesh with collagen sponge, which were designed for inducing tissue invasion into the material.[4-7] Collagen sponge provides not only air sealing but also enhancement of tissue invasion into the material. A Y-shaped tracheal prosthesis was implanted, and tracheal tissue was successfully regenerated in animal experiments, as well as with a straight-type tracheal prosthesis.

Tissue engineering technology consists of three factors: scaffold, cells, and regulation factors.[8] Highly differentiated tissues and organs are able to regenerate under the appropriate conditions. In situ tissue engineering of the trachea, esophagus, stomach, and intestine has been studied by implantation of collagen sponge as a scaffold graft without additional cells or outside regulation factors.[4-7,9-11] According to the results, the collagen sponge scaffold could provide favorable conditions for tissue regeneration in vivo in combination with infiltrated host cells and regulation factors released during the inflammatory process. It has been reported that collagen, which is a component of the extracellular matrix, induces cell transformation, division, proliferation, and detachment.[13] During repair of injured tissues and organs, endogenous factors are naturally secreted at damaged sites as regulation factors.[14]

In our experimental studies, histologic findings showed good incorporation of the scaffold mesh into the host tissue and regeneration of the ciliated epithelium over the mesh tube. Mechanical tests demonstrated that the regenerated tissue firmly supported the airway framework for respiration. The Marlex mesh tube with collagen provided a good environment for regenerating the subglottic and tracheal epithelium without the addition of cells or outside regulation factors.

On the basis of successful experimental studies, this newly developed method for regeneration of the tracheal tissue was applied to a human patient. In this case, the right half of three rings of the trachea was resected. The defect was not too large for use of the conventional techniques; however, the current regenerative technique avoided tracheotomy, a second operation, and deformity. Good epithelialization has been observed on the tracheal luminal surface without any complications for 2 years (as of January 2005). Although long-term follow-up is required, in situ tissue engineering of the tracheal tissue is feasible and practical after resection of the trachea with airway lesions of malignancies or stenosis.

REFERENCES

1. Cotton RT. Management of subglottic stenosis. Otolaryngol Clin North Am 2000;33:111-30.

2. Caputo V, Consiglio V. The use of patient's own auricular cartilage to repair deficiency of the tracheal wall. J Thorac Cardiovasc Surg 1961;41:594-6.

3. Neville WE, Bolanowski PJ, Kotia GG. Clinical experience with the silicone tracheal prosthesis. J Thorac Cardiovasc Surg 1990;99:604-13.

4. Teramachi M, Kiyotani T, Takimoto Y, Nakamura T, Shimizu Y. A new porous tracheal prosthesis sealed with collagen sponge. ASAIO J 1995;41:M306-M310.

5. Teramachi M, Nakamura T, Yamamoto Y, Kiyotani T, Takimoto Y, Shimizu Y. Porous-type tracheal prosthesis sealed with collagen sponge. Ann Thorac Surg 1997;64:965-9.

6. Teramachi M, Okumura N, Nakamura T, et al. Intrathoracic tracheal reconstruction with a collagen-conjugated prosthesis: evaluation of the efficacy of omental wrapping. J Thorac Cardiovasc Surg 1997;113:701-11.

7. Nakamura T, Teramachi M, Sekine T, et al. Artificial trachea and long term follow-up in carinal reconstruction in dogs. Int J Artif Organs 2000;23:718-24.

8. Bianco P, Robey PG. Stem cells in tissue engineering. Nature 2001;414:118-21.

9. Yamamoto Y, Nakamura T, Shimizu Y, et al. Intrathoracic esophageal replacement in the dog with the use of an artificial esophagus composed of a collagen sponge with a double-layered silicone tube. J Thorac Cardiovasc Surg 1999;118:276-86.

10. Hori Y, Nakamura T, Matsumoto K, Kurokawa Y, Satomi S, Shimizu Y. Experimental study on in situ tissue engineering of the stomach by an acellular collagen sponge scaffold graft. ASAIO J 2001;47:206-10.

11. Hori Y, Nakamura T, Matsumoto K, Kurokawa Y, Satomi S, Shimizu Y. Tissue engineering of the small intestine by acellular collagen sponge scaffold grafting. Int J Artif Organs 2001; 24:50-4.

12. Omori K, Nakamura T, Kanemaru S, et al. Cricoid regeneration using in situ tissue engineering in canine larynx for the treatment of subglottic stenosis. Ann Otol Rhinol Laryngol 2004; 113:623-7.

13. Breuing K, Andree C, Helo G, Slama J, Liu PY, Eriksson E. Growth factors in the repair of partial thickness porcine skin wounds. Plast Reconstr Surg 1997;100:657-64.

14. Ruoslahti E, Hayman EG, Pierschbacher MD. Extracellular matrices and cell adhesion. Arteriosclerosis 1985;5:581-94.

Annals of Otology, Rhinology & Laryngology 115(1):23-29.

Morphological and Histologic Examination of the Epiglottis: Implications for Improving Epiglottic Closure Technique

Shuji Yokoyama, MD; Makoto Kano, MD; Mutsumi Watanabe, MD; Hiroshi Ogawa, MD; Koichi Omori, MD

Objectives: We conducted a histologic examination and measured the tension on the epiglottis to determine how dehiscence of the epiglottis can be prevented after epiglottic closure surgery.

Methods: We classified configurations of the epiglottis into flat, intermediate, and omega types and studied the histology of each type. We also measured the tension in each of these 3 morphological types on 4 regions of the epiglottis (upper, middle, and lower points, and the cuneiform tubercle) at 3 different times: before incision, after median incision, and after reversed-Y incision.

Results: No histologic differences were evident among the epiglottic types. In the flat and intermediate types, the tension measured before incision decreased significantly upon completion of the median incision at every point. In these 2 types, the reversed-Y incision resulted in a further significant decrease in tension at the middle and lower points. In the omega type, the tension was low before incision and was not significantly reduced by either incision.

Conclusions: We demonstrated that a median incision alone effectively decreased tension sufficiently to prevent dehiscence. The reversed-Y incision was even more effective for decreasing tension at the middle and lower points.

Key Words: aspiration pneumonia, epiglottic cartilage, epiglottic closure, epiglottis.

INTRODUCTION

A variety of surgical procedures can prevent refractory aspiration pneumonia. One such procedure, first performed by Biller et al,[1] involves suturing the epiglottis into a rolled state to prevent aspiration after total glossectomy. The tip of the epiglottis remains unsutured, leaving a small opening so that phonation can be preserved. We perform epiglottic closure (a modification of the method of Biller et al), as described in case reports by Tanabe et al,[2] in patients with dysphagia associated with cerebrovascular disease or neuromuscular disorders or with dysphagia that occurred as a postoperative complication of cerebral tumor excision. Phonation can be easily achieved after this surgical technique by closing the stoma with the finger during expiration, although a permanent tracheostoma is necessary. Furthermore, this procedure is advantageous because ingestion can begin without preparatory exercises for deglutition. However, it is well known that postoperative dehiscence of the sutured epiglottis sometimes occurs even though no failure has been noted. In our experience, epiglottal dehiscence has occurred in 3 of 9 cases, and repeat surgery was required. We therefore conducted a histologic examination and measured tension on the epiglottis to determine how dehiscence of the epiglottis following epiglottic closure can be prevented.

MATERIALS AND METHODS

MORPHOLOGICAL AND HISTOLOGIC STUDY OF EPIGLOTTIC CARTILAGE

For this morphological and histologic study of epiglottic cartilage, autopsies were conducted at Fukushima Medical University School of Medicine. Laryngeal specimens were removed from male cadavers with no evidence of laryngeal lesions and were examined histologically. In order to compare histologic characteristics across morphologically different forms of the epiglottis, we examined 3 specimens of each type of epiglottis (flat type, intermediate type, and omega [Ω] type; defined below) taken at autopsy from subjects between 60 and 69 years of age. In order to assess the effect of age on the histologic characteristics of the epiglottis, we examined 3 autopsy

From the Department of Otolaryngology, Fukushima Medical University School of Medicine, Fukushima City, Japan. This study was supported in part by a grant from Health and Labor Science Research Grants for Research on Human Genome, Tissue Engineering, from the Ministry of Health, Labor and Welfare.

Presented at the meeting of the American Laryngological Association, Boca Raton, Florida, May 13-14, 2005. Dr Yokoyama received the Second Place Award for poster presentations for 2005 from the Association.

Correspondence: Koichi Omori, MD, Dept of Otolaryngology, Fukushima Medical University School of Medicine, 1 Hikarigaoka, Fukushima City, Fukushima, 960-1247, Japan.

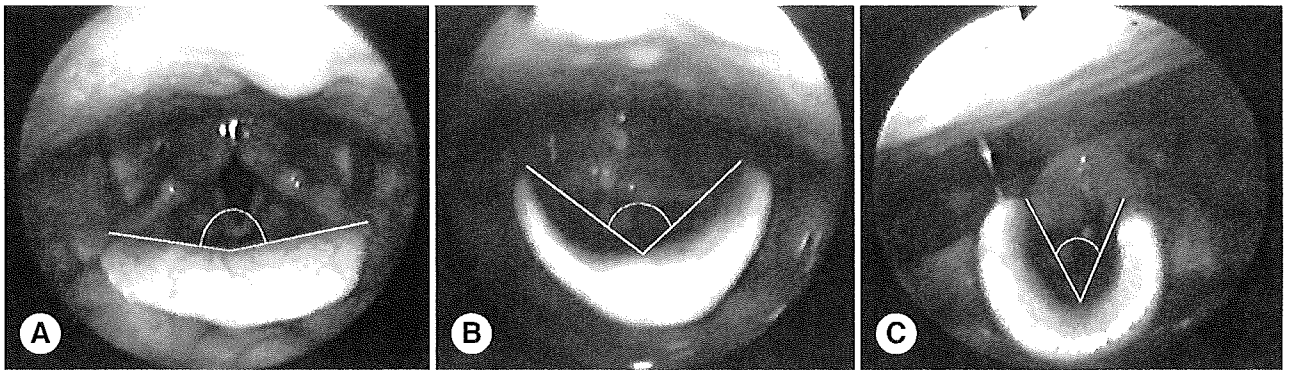

Fig 1. Classification of epiglottis form. **A)** Flat type. **B)** Intermediate type. **C)** Omega type.

specimens of flat-type epiglottis in each of the age groups 20 to 29 years, 40 to 49 years, and 60 to 69 years. After paraffin embedding, thin sections were taken from the upper, middle, and lower regions of the epiglottis. At each region, cartilage ossification, chondrocyte appearance and number, and proportions of elastic fibers and acid mucopolysaccharide were observed under light microscopy with use of hematoxylin and eosin, elastica-Masson, and Alcian blue stains.

CLASSIFICATION OF EPIGLOTTIC FORM AND METHOD OF TENSION MEASUREMENT

Next, to investigate the relationship between epiglottic form and tension, we extirpated and examined the larynges of 18 male patients, ranging in age from 42 to 77 years, in whom carcinoma of the oral, pharyngeal, or laryngeal structures was diagnosed. The morphological forms of the epiglottis were classified into the following 3 types: flat, intermediate, and omega. The angle formed by the center of the epiglottis and the incline of the left and right aryepiglottic folds was more than 120° in the flat type (n = 8), between 60° and 120° in the intermediate type (n = 5), and less than 60° in the omega type (n = 5; Fig 1). In all types, the epiglottis was divided into 4 equal regions from the tip to the cuneiform tubercle to establish 4 measurement points: upper, middle, lower, and cuneiform tubercle (Fig 2A). A silk thread was pulled through the peripheral region of the left and right parts of the epiglottic cartilage at each point and tightened to bring the parts into contact at the median line (Fig 2B). The amount of tension placed on these threads was measured at 3 different times: before the incision, after placing a vertical incision along the median line of the epiglottic cartilage (median incision; Fig 3), and after extending the median incision inferolaterally into an upside-down Y–shaped incision (reversed-Y incision). All measurements were made with a force gauge meter (A&D Engineering, Inc, Milpitas, California) and are shown as absolute values.

RESULTS

HISTOLOGIC EXAMINATION OF EPIGLOTTIC CARTILAGE

Comparison Among Age Groups. Ossification of the epiglottic cartilage was recognized in all 3 samples from subjects in their sixties, and partial ossification was apparent in all 3 samples from subjects in their twenties (Fig 4). Chondrocytes in specimens from subjects 60 to 69 years of age demonstrated less uniformity of size and more numerous vacuoles than those from subjects 20 to 29 years of age. On the other hand, no difference in the proportion of elas-

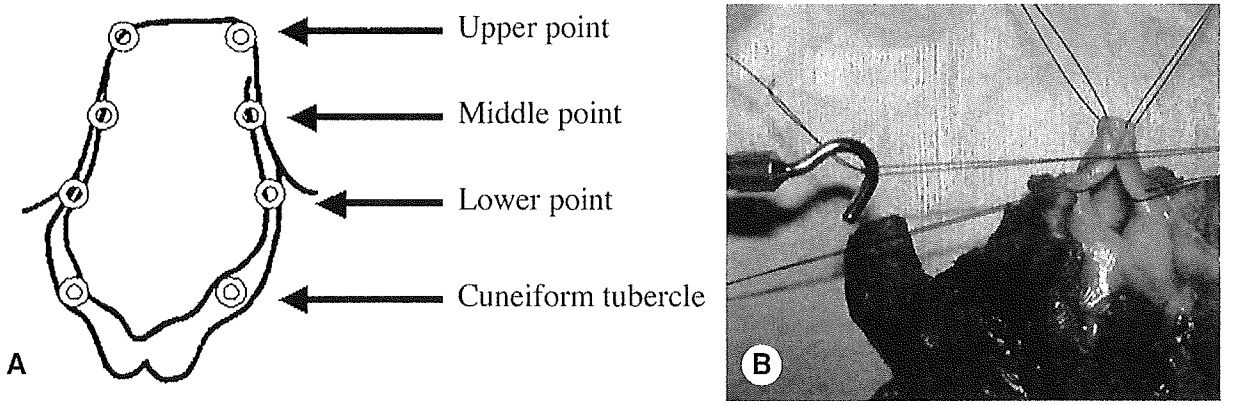

Fig 2. Measurement of tension on epiglottis. **A)** Measurement points. **B)** Method of measurement.

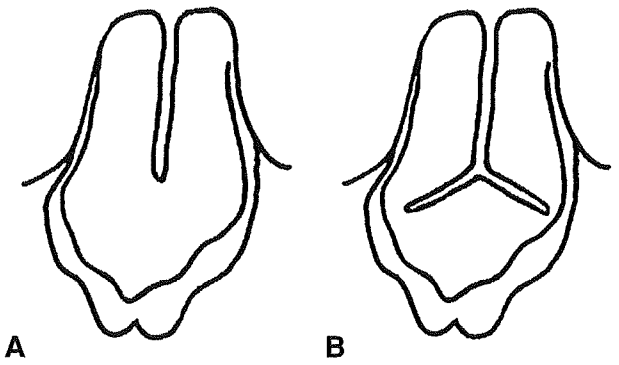

Fig 3. Schema of epiglottic incisions. **A)** Median incision. **B)** Reversed-Y incision.

tic fibers was noted between the two groups. In addition, no differences in ossification or in the proportion of elastic fibers were evident between subjects 60 to 69 years of age and those 40 to 49 years of age. The amount of acid mucopolysaccharide, the main constituent of cartilage matrix, decreased with aging.

Comparison Among Morphological Types. On comparison of epiglottic tissue from subjects within the same age group, we found that the number of chondrocytes, the degree of ossification, and the number of elastic fibers were similar across all types. However, levels of acid mucopolysaccharide were reduced in the middle region of the omega-type epiglottis as compared with those measured in the flat type and the intermediate type (Fig 5).

TENSION ON EPIGLOTTIS

Comparison of Tension Among Flat, Intermediate, and Omega Epiglottis Types Before Incision. For the flat, intermediate, and omega types of epiglottis from the excised larynges, the mean tensions at 4 points are shown in Table 1 and Fig 6. At the upper, middle, and lower points, but not at the cuneiform tubercle, the tension differed significantly between the flat type and the intermediate type ($p < .05$), between the intermediate type and the omega type ($p < .05$), and between the flat type and the omega type ($p < .05$).

Comparison of Tension With Respect to Type of Incision in Flat-Type Epiglottis. In the flat-type epiglottis (Table 2, Fig 7A), the mean tension significantly decreased from before incision to after completion of the median incision at the upper, middle, and lower points ($p < .01$). Although the tension decreased at the cuneiform tubercle, the decrease was not significant. The mean tension significantly decreased further upon completion of the reversed-Y incision at the upper, middle, and lower points ($p < .01$). Although the tension decreased at the cuneiform tubercle, the decrease was not significant.

Comparison of Tension With Respect to Type of Incision in Intermediate-Type Epiglottis. In the intermediate-type epiglottis (Table 3, Fig 7B), the mean tension significantly decreased from before to after completion of the median incision at the upper, middle, and lower points ($p < .01$). The mean tension significantly decreased further upon completion of the reversed-Y incision at the middle and lower points ($p < .01$). There was a significant difference in the tension between before the incision and after the reversed-Y incision at the upper, middle, and lower points.

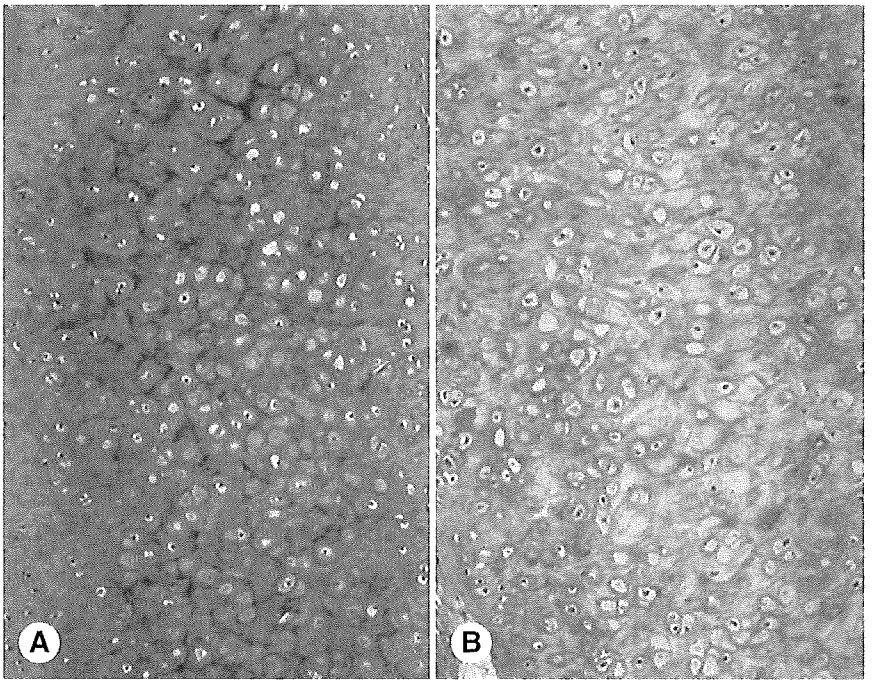

Fig 4. Histologic examination of epiglottic cartilages (H & E, original ×100). **A)** Example from group 20 to 29 years of age. **B)** Example from group 60 to 69 years of age.

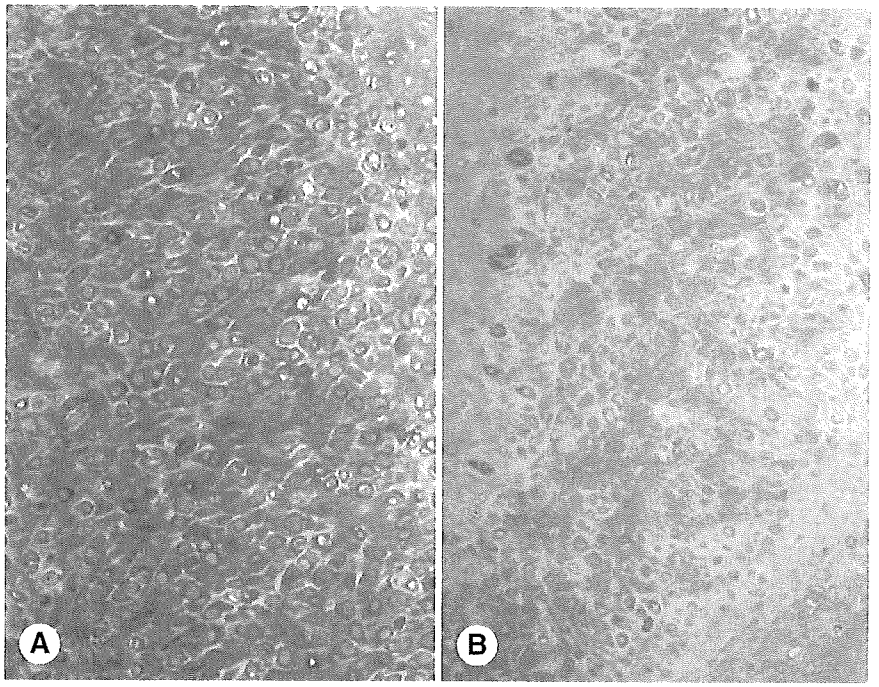

Fig 5. Histologic examination of epiglottic cartilages (Alcian blue stain, original ×100). **A)** Flat type. **B)** Omega type.

Comparison of Tension With Respect to Type of Incision in Omega-Type Epiglottis. In the omega-type epiglottis (Table 4, Fig 7C), although the mean tension decreased from before the incision to after the completion of the median incision at all points, the decrease was not significant. The mean tension decreased further upon completion of the reversed-Y incision at all points, but there was no significant difference.

DISCUSSION

The most reliable surgical intervention for central dysphagia is laryngeal closure or total laryngectomy, or tracheoesophageal diversion.[3] We performed epiglottic closure (a modification of the method of Biller et al[1]) to prevent aspiration in cases of central dysphagia and to preserve phonation in order to maintain patient quality of life. However, epiglottal dehiscence occurred in 3 of 9 cases (in the upper region in 1 patient; in both the middle and lower regions in 2 patients), and repeat surgery was required. Meiteles et al[4] reported that making an additional vertical incision in the epiglottic cartilage prevents postoperative dehiscence. Another reported method of avoiding this complication involves breaking the thyroid cartilage at the midline.[5] In the present study, we examined the effects of aging and of epiglottic configuration on epiglottic histology. We also investigated the relationship between the morphological form of the epiglottic cartilage and the tension that results from suturing this elastic structure, and the effect of the type of incision on this tension.

TABLE 1. MEAN TENSION AMONG FLAT, INTERMEDIATE, AND OMEGA TYPES OF EPIGLOTTIS BEFORE INCISION

Measurement Point	*Flat (g)*	*Intermediate (g)*	*Omega (g)*
Upper	74.6 ± 30.1	32.6 ± 8.0	12.0 ± 5.1
Middle	125.6 ± 18.2	59.8 ± 22.1	12.8 ± 4.8
Lower	124.6 ± 23.0	73.8 ± 12.9	7.2 ± 3.8
Cuneiform tubercle	16.9 ± 8.1	17.2 ± 5.9	6.8 ± 3.2

Data are mean ± SD.

HISTOLOGY OF EPIGLOTTIS

The epiglottis is histologically composed of elastic cartilage; the only other sites at which this tissue is found are the auricle and the external auditory meatus. It was previously thought that elastic cartilage

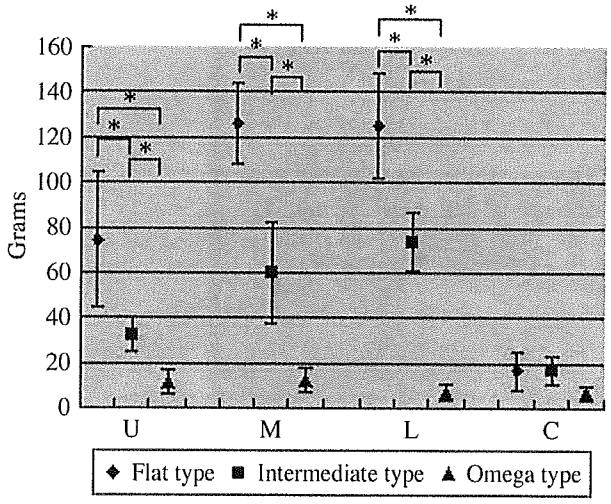

Fig 6. Tension on 3 types before incision at each measurement point. U — upper; M — middle; L — lower; C — cuneiform tubercle; asterisks — $p < .05$.

TABLE 2. COMPARISON OF MEAN TENSION WITH RESPECT TO TYPE OF INCISION IN FLAT-TYPE EPIGLOTTIS

		After Incision			
		Median Incision		*Reversed-Y Incision*	
Measurement Point	*Before Incision (g)*	*g*	*% Decrease*	*g*	*% Decrease*
Upper	74.6	25.5	65.8	4.5	43.1
Middle	125.6	37.1	70.5	21.1	43.1
Lower	124.6	51.5	58.7	24.0	53.4
Cuneiform tubercle	16.9	12.1	28.4	10.1	16.5

TABLE 3. COMPARISON OF MEAN TENSION WITH RESPECT TO TYPE OF INCISION IN INTERMEDIATE-TYPE EPIGLOTTIS

		After Incision			
		Median Incision		*Reversed-Y Incision*	
Measurement Point	*Before Incision (g)*	*g*	*% Decrease*	*g*	*% Decrease*
Upper	32.6	15.2	53.4	12.0	21.1
Middle	59.8	28.2	52.8	14.8	47.5
Lower	73.8	35.4	52.0	15.0	57.6
Cuneiform tubercle	17.2	12.2	29.1	10.4	14.8

rarely undergoes ossification or degeneration similar to that seen in asbestosis.[6] However, ossification of epiglottic cartilage was documented by Endo,[7] who reported that cartilage at this site is immature for the first 3 months after birth, begins to ossify at 30 years of age, and exhibits chondrocyte vacuolation and marked ossification after 50 years of age. Rother and Rodel[8] reported that the number of chondrocytes in the epiglottic cartilage decreases rapidly through the age of 10 years and continues to fall with age. In the current study, chondrocyte size became less uniform and vacuolation increased with aging in all types of epiglottis. Among specimens from cadavers within the same age group, no differences in the proportion of elastic fibers or the degree of ossification were observed among the flat, intermediate, and omega types. Alcian blue staining demonstrated that acid mucopolysaccharide levels decreased slightly in the middle region of the cartilage in the omega-type epiglottis from subjects in their sixties, and that the amount of acid mucopolysaccharide decreased with age. The occasionally encountered condition of flaccid epiglottis (floppy epiglottis) demonstrates similar histologic findings, and it is assumed that acid mucopolysaccharide levels in the cartilage tissue are low in this condition.[9] The epiglottis can also under-

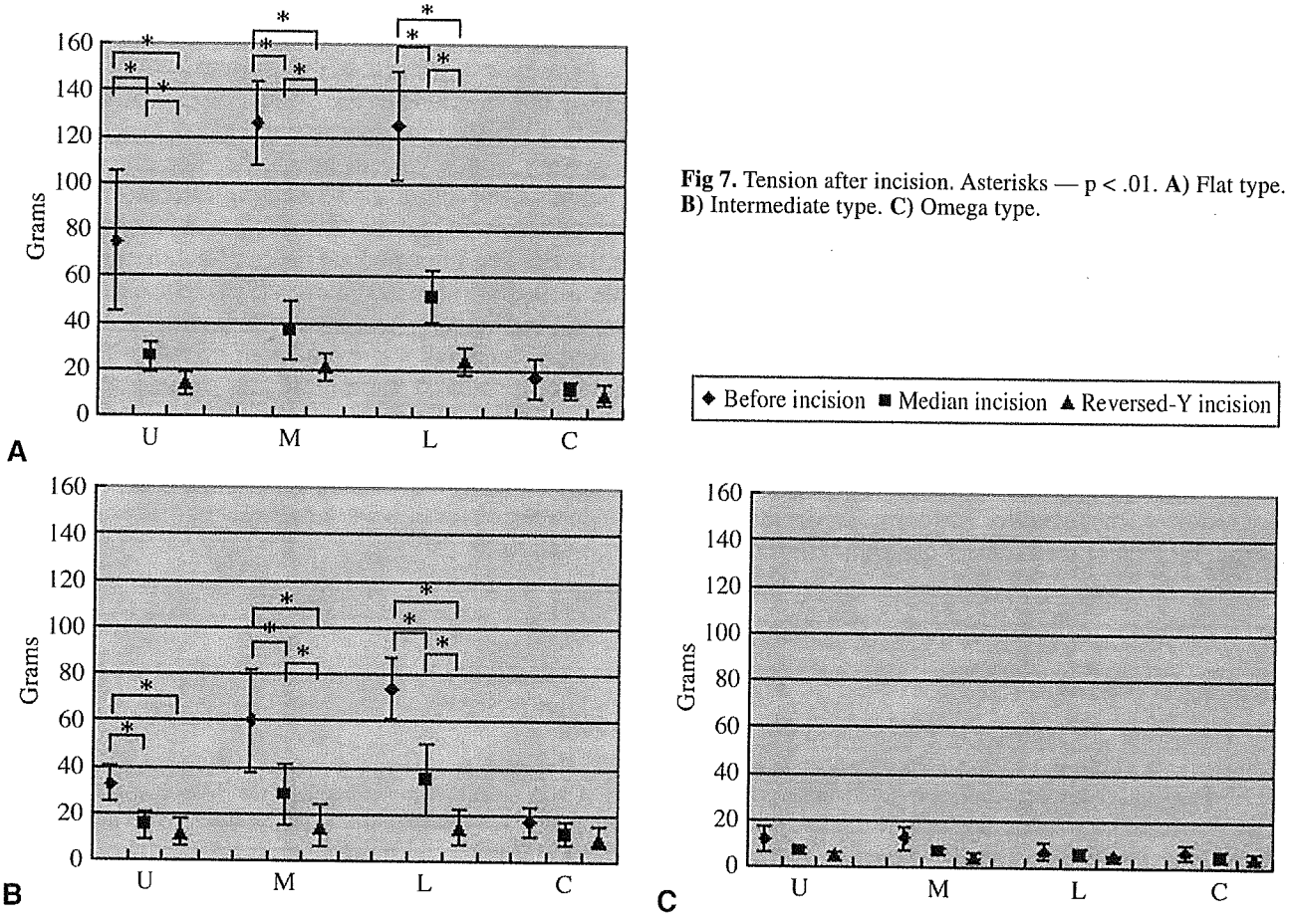

Fig 7. Tension after incision. Asterisks — $p < .01$. **A)** Flat type. **B)** Intermediate type. **C)** Omega type.

TABLE 4. COMPARISON OF MEAN TENSION WITH RESPECT TO TYPE OF INCISION IN OMEGA-TYPE EPIGLOTTIS

		After Incision			
		Median Incision		Reversed-Y Incision	
Measurement Point	Before Incision (g)	g	% Decrease	g	% Decrease
Upper	12.0	6.8	43.3	5.0	26.5
Middle	12.8	6.8	46.9	4.6	32.4
Lower	7.2	6.0	16.7	5.0	16.7
Cuneiform tubercle	6.8	5.0	26.9	4.5	10.0

go atrophy and deformity as a result of perichondritis; however, this process involves histologic changes different from those observed in the present study.[10]

RELATIONSHIP BETWEEN EPIGLOTTIC FORM AND TENSION BEFORE INCISION

A variety of morphological forms of the epiglottis exist, although only 3 types were examined in the present study, with the same number of samples for each. The tension on the flat type was significantly higher at the upper (6 times), middle (10 times), and lower points (17 times) than that observed on the omega type. In addition, the tension on the intermediate type was 5 to 10 times higher at the middle and lower points than that observed on the omega type. On the other hand, in both groups, the tension was low at the cuneiform tubercle (15 g or less; no significant difference). This finding suggests that the elasticity of the cartilage is low in both morphological types at this point. The tension was more than 100 g in the flat type at the upper point, and was particularly high at the middle and lower points, the sites at which dehiscence becomes a clinical problem.

DECREASED TENSION INDUCED BY INCISION OF EPIGLOTTIC CARTILAGE

Flat Type. The median incision was effective in significantly decreasing the mean tension, which decreased by as much as 25 g at the upper point and by as much as 50 g at the middle and lower points upon completion of this incision. Furthermore, the tension significantly decreased further on completion of the reversed-Y incision, by as much as 15 g at the upper point and as much as 25 g at the middle and lower points. Diminished tension was particularly conspicuous at the middle and lower points, indicating that the reversed-Y incision was a useful surgical procedure. On the other hand, the decrease in tension was negligible at the cuneiform tubercle.

Intermediate Type. In this morphological form, the tension at the middle and lower points was high, and the reversed-Y incision resulted in a significant decrease in tension at these points. However, the decrease in tension was negligible at the cuneiform tubercle.

Omega Type. Before any incision, the mean tension was 15 g or less (ie, similar to baseline value) in this type of cartilage, and neither the median incision nor the reversed-Y incision significantly decreased tension. We therefore believe that there are few advantages to incising the epiglottic cartilage in patients with this morphological type of epiglottis.

CLINICAL APPLICATIONS: ADAPTATION OF SURGICAL PROCEDURE TO DECREASE TENSION

We observed an obvious difference between the tension on the epiglottis during surgery and the morphological form of the epiglottis. Accordingly, clinicians should consider the morphology of the patient's epiglottis when deciding whether to use the modified surgical technique to prevent dehiscence. This consideration is particularly important in light of our results in patients with the omega type, which indicate that incision for decreasing tension may be unnecessary in this type of epiglottis. The amount of tension varied according to the epiglottic region and was particularly high at the middle and lower points of the flat and intermediate types. We demonstrated that a median incision alone effectively decreased tension sufficiently to prevent dehiscence. The reversed-Y incision was even more effective for decreasing tension at the middle and lower points. In the present study, we found it useful to perform the reversed-Y incision in order to prevent dehiscence in the flat and intermediate types, whereas incision for decreasing tension was unnecessary in the omega-type epiglottis.

REFERENCES

1. Biller HF, Lawson W, Baek SM. Total glossectomy. A technique of reconstruction eliminating laryngectomy. Arch Otolaryngol 1983;109:69-73.

2. Tanabe M, Katsumi Y, Ohnishi K, Ishikawa M, Kanemaru S, Shigematsu A. A surgical treatment for aspiration preserving phonatory function. J Jpn Bronchoesophagol Soc 1992;43:348-52.

3. Lindeman RC. Diverting the paralyzed larynx: a reversible procedure for intractable aspiration. Laryngoscope 1975;85: 157-80.

4. Meiteles LZ, Kraus W, Shemen L. Modified epiglottoplasty for prevention of aspiration. Laryngoscope 1993;103: 1395-8.

5. Terada A, Hasegawa Y, Fujimoto Y, Matsuura H, Takahashi M, Nakajima T. A modification of the Biller et al method of laryngoplasty for major glossectomy in elderly patients. Pract Otologica (Kyoto) 1999;92:509-11.

6. Cox RW, Peacock MA. The fine structure of developing

elastic cartilage. J Anat (Lond) 1977;123:283-96.

7. Endo N. Histological study on the larynx: its histological change with increasing age. J Jpn Bronchoesophagol Soc 1972;23:322-44.

8. Rother P, Rodel P. Stereologische Untersuchungen zum Alternswandel der Knorpelzellen der Epiglottis. Z Mikrosk Anat Forsch 1975;89:839-58.

9. Tanaka F, Haji T, Shinjo Y, Maeda H, Takebayashi S, Yagi N. Hyperventilation syndrome in flaccid epiglottis. Otologia Fukuoka 1996;42:354-7.

10. Aoki K. Relapsing polychondritis. J Adult Dis 1993;23: 1760-3.

Conversion of aquaporin 6 from an anion channel to a water-selective channel by a single amino acid substitution

Kun Liu*, David Kozono*, Yasuhiro Kato†, Peter Agre*‡, Akihiro Hazama§, and Masato Yasui*¶‖

Departments of *Biological Chemistry, ‡Medicine, and ¶Pediatrics, The Johns Hopkins University School of Medicine, Baltimore, MD 21205; †Cornea Center, Tokyo Dental College, Ichikawa, Chiba 272-8513, Japan; and §Department of Physiology, Fukushima Medical College, Fukushima 960-1295, Japan

Contributed by Peter Agre, December 21, 2004

Aquaporin (AQP) 6 belongs to the aquaporin water channel family. Unlike other aquaporins, AQP6 functions not as a water channel but as an anion-selective channel. Single-channel analyses have shown AQP6 to flicker rapidly between closed and open status. The atomic structure of AQP1 and amino acid sequence alignments of the mammalian aquaporins reveal two well conserved glycine residues: Gly-57 in transmembrane helix (TM) 2 and Gly-173 in TM5 reside at the contact point where the two helices cross in human AQP1. Uniquely, all known mammalian orthologs of AQP6 have an asparagine residue (Asn-60) at the position corresponding to Gly-57. Here we show that a single residue substitution (N60G in rat AQP6) totally eliminates the anion permeability of AQP6 when expressed in *Xenopus* oocytes, but the N60G oocytes exhibit significantly higher osmotic water permeability under basal conditions. Replacement of the glycine at this site in AQP0, AQP1, and AQP2 blocked expression of the mutants at the oocyte plasma membrane. We propose that the asparagine residue at the contact point between TM2 and TM5 in AQP6 may function as a teeter board needed for rapid structural oscillations during anion permeation.

anion permeability | structure–function | water permeability

The aquaporins are a family of integral membrane proteins that function largely as water channels at the plasma membranes of cells (1). Ion permeability, including hydronium ions, is not a general feature of aquaporins (2–7). We recently demonstrated, however, that aquaporin (AQP) 6 functions not as a water channel but as an anion channel with the halide permeability sequence: $NO_3^- > I^- \gg Br^- > Cl^- \gg F^-$ (8, 9). When expressed in *Xenopus laevis* oocytes, AQP6 exhibited minimal water permeability. In mammalian cells expressing GFP-tagged AQP6, outward rectifying currents were induced after replacing NaCl with $NaNO_3$ in the bath solution. Moreover, we showed that AQP6 is a gated channel by single-channel patch recording with oocyte membranes expressing AQP6 (10). The unique functions of AQP6 may be due to its distinct structure, especially in the formation of its pore.

The atomic structure of AQP1 has been established by electron crystallography and x-ray crystallography (11, 12). AQP1 exists as a tetramer with each subunit containing its own pore. The hourglass-shaped pore is formed by two loops, each containing a highly conserved NPA motif and a short helix and by a right-handed bundle of six highly tilted α-helices. There are three sites where helices cross, between helices 1 and 3, 4 and 6, and 2 and 5. All three have highly conserved glycine residues at the contact sites, and this is thought to stabilize the monomer (13). The atomic structure and molecular dynamics simulations of AQP1 provide a uniquely selective mechanism for free permeation by water through the channel pore and a mechanism for proton blockage: (*i*) size restriction at the narrowest constriction of the pore; (*ii*) electrostatic repulsion by the well conserved arginine residue right after the second NPA motif; and (*iii*) water dipole reorientation at the midpoint of the pore, which disrupts hydrogen bonding in the single-file chain of water molecules (14). The amino acid sequence of AQP6 reveals that AQP6 potentially meets these mechanisms despite limited water permeability under basal conditions (15–17). AQP6 contains most of the conserved amino acid residues, including the NPA motifs. Also, the structure of AQP1 does not reveal mechanisms for gating, although most ion channels have well characterized gating mechanisms. Careful analysis of aquaporin sequence alignments with insight provided by structural models led us to identify a critical amino acid residue for anion permeability by AQP6.

Table 1. Site-directed mutations

	WT		Mutant	
Mutation	Amino acid	Codon	Amino acid	Codon
AQP6 N60G	Asn-60	AAC	Gly-60	GGC
AQP6 N60G/G174N	Asn-60	AAC	Gly-60	GGC
	Gly-174	GGG	Asn-174	AAC
AQP0 G49N	Gly-49	GGC	Asn-49	AAC
AQP1 G57N	Gly-57	GGG	Asn-57	AAC
AQP2 G49N	Gly-49	GGT	Asn-49	AAT

Materials and Methods

Sequence Alignment and Structural Model. Amino acid sequences of *Rattus norvegicus* (rat) AQP0 (P09011), AQP1 (NP_036910), AQP2 (NP_037041), AQP4 (NP_036957), AQP5 (NP_036911), and AQP6 (NP_071517) were aligned with CLUSTALX (Ver. 1.83). Regions containing transmembrane helix (TM) 2 and TM5 were selected based on x-ray crystallographic topology of AQP1 (12). The modeled structure of rat AQP6 was based on bovine AQP0, the most highly homologous sequence to AQP6 with a published atomic structure (18). The N-terminal 12- and C-terminal 28 amino acid residues of AQP6 were removed, because these two fragments do not have counterparts in AQP0 structure. Modeling was performed by the program JACKAL (http://trantor.bioc.columbia.edu/programs/jackal). Figures were prepared and rendered by SPDBV (3.7.5) or PYMOL (www.pymol.org).

Plasmid Construction. pXβG-ev1-AQP6 N60G, N60G/G174N, pXβG-ev1-AQP0 G49N, -AQP1 G57N, or -AQP2 G49N mutant was constructed with the QuikChange site-directed mutagenesis kit (Stratagene). Templates were pXβG-ev1-AQP6, -AQP0, -AQP1, or -AQP2. Table 1 lists the mutants used in this study. Mutations were confirmed by sequencing.

Abbreviations: AQP*n*, aquaporin *n*; TM*n*, transmembrane helix *n*.

See Commentary on page 1813.

To whom correspondence should be addressed. E-mail: myasui@jhmi.edu.

www.pnas.org/cgi/doi/10.1073/pnas.0409232102

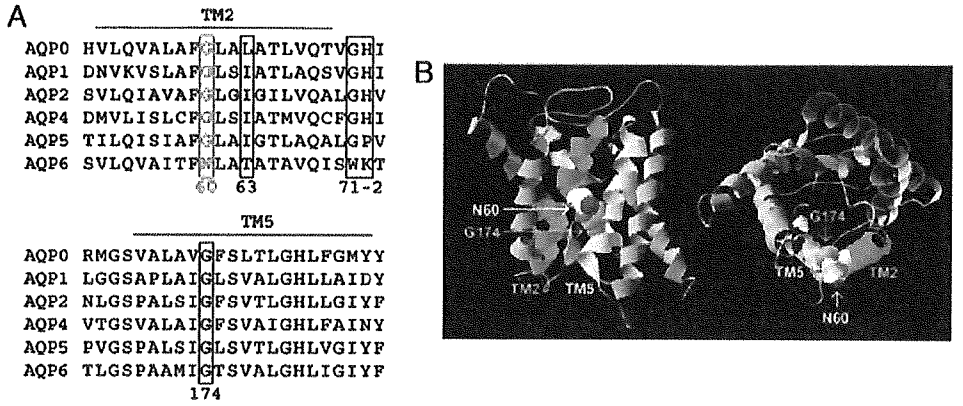

Fig. 1. Unique residues in AQP6 structure. (*A*) Sequence alignment of TM2 and TM5 of rat aquaporin proteins in the water-selective subgroup. Key residues implicated in AQP6 anion conductance including Asn-60, Thr-63, Trp-71, and Lys-72 are indicated in rectangles and numbered based on position in rat AQP6. (*B*) Structural model of AQP6, based on threading through the atomic structure of AQP0 (18). Two views, sagittal (*Left*) and cross-sectional (*Right*), highlighting the interaction between TM2 (in green) and TM5 (in orange), are shown in ribbon form. The side chain of Asn-60 is depicted with van der Waals space-filling spheres in CPK colors. The backbone atoms of Gly-174 are depicted with van der Waals space-filling spheres in magenta.

Expression in Oocytes and Measurement of P_f. Capped cRNAs were synthesized *in vitro* from *Xba*I-linearized pXβG -ev1 plasmids by using T3 RNA polymerase and purified with the RNeasy Mini kit from Qiagen (Valencia, CA). Defolliculated *X. laevis* oocytes were injected with 5 or 15 ng of cRNA or 50 nl of diethyl pyrocarbonate-treated water. Injected oocytes were incubated

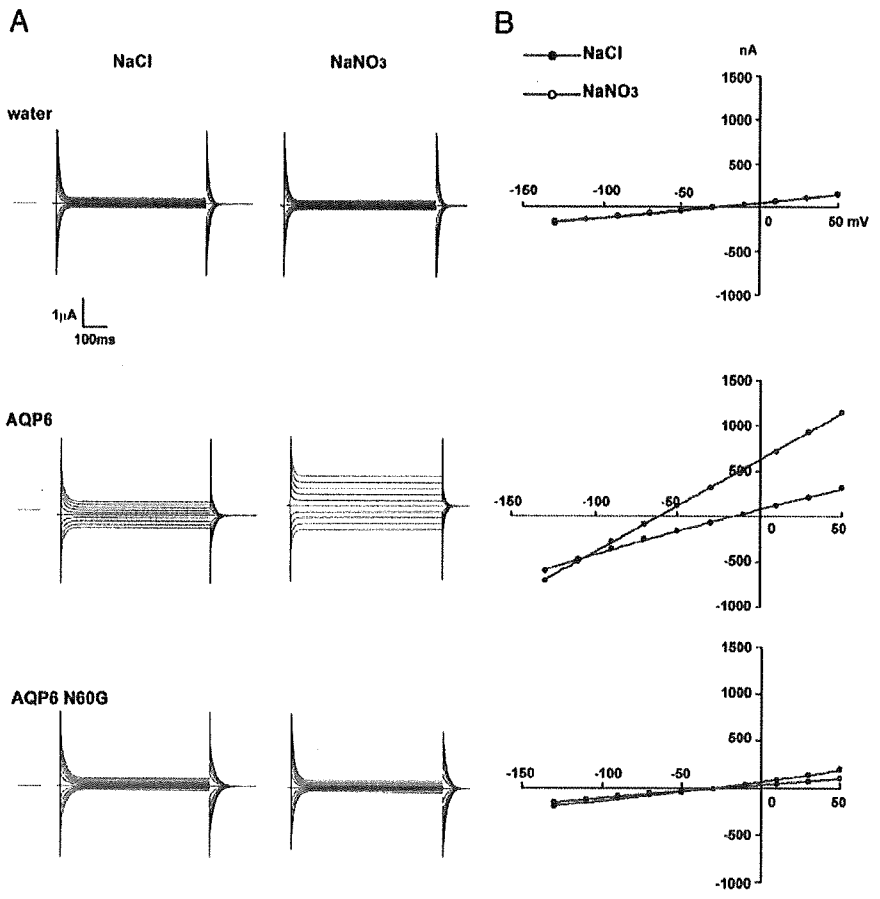

Fig. 2. Electrophysiological analyses of AQP6 and N60G. (*A*) Representative currents of water-injected oocytes (*Top*), AQP6 oocytes (*Middle*), and N60G oocytes (*Bottom*) under NaCl solution (*Left*) and $NaNO_3$ solution (*Right*). The membrane potential was held at −50 mV and jumped to test potentials from +50 mV to −130 mV with 20 mV step voltage. The dashed line indicates the zero current level. (*B*) Representative I–V curves of water-injected oocyte (*Top*), AQP6 oocyte (*Middle*), and N60G oocyte (*Bottom*) in NaCl solution (open circles) or $NaNO_3$ solution (filled circles).

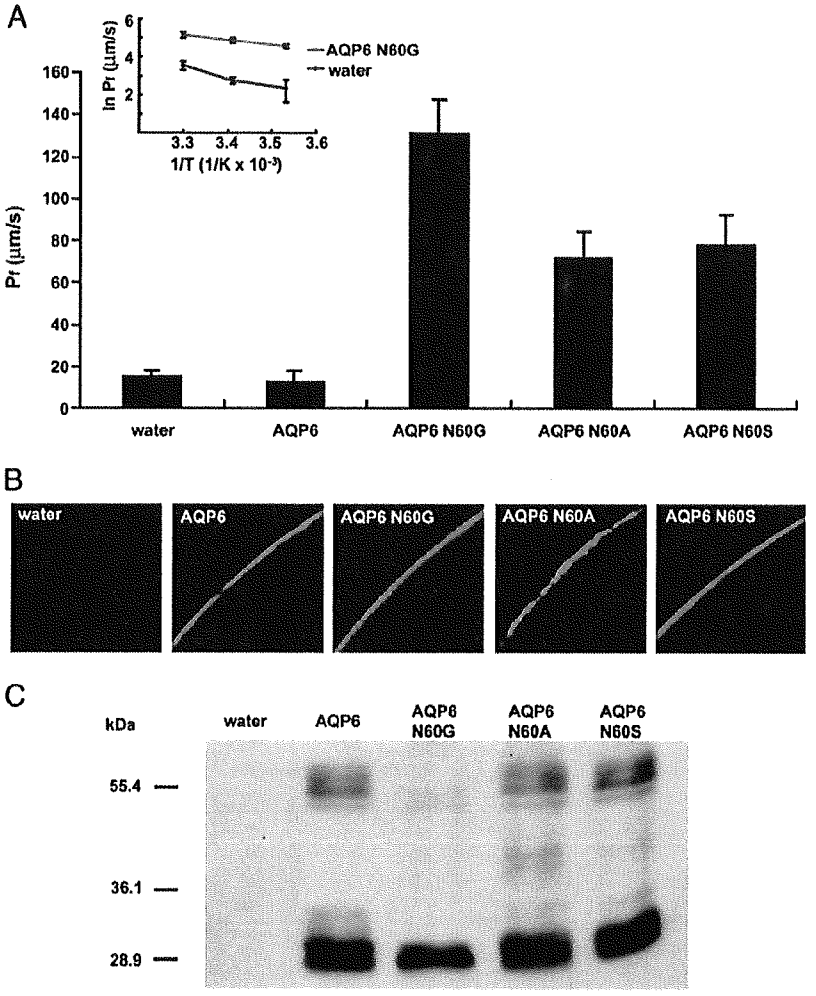

Fig. 3. Rat AQP6 or mutants expressed in oocytes. *X. laevis* oocytes were injected with 15 ng of AQP6 WT, N60G, N60A, or N60S cRNA and cultured for 2.5 days. (*A*) Osmotic water permeability (P_f) of AQP6 or mutants. Arrhenius activation energy (E_a) of osmotic water permeabilities of N60G mutant oocytes and water-injected control oocytes (*Inset*). Osmotic-swelling assays were performed at 10, 20, or 30°C (mean ± SD, $n = 5$). (*B*) Confocal microscopy of oocytes injected with water, AQP6 WT, N60G, N60A, or N60S cRNA. The oocytes were stained by anti-rat AQP6 antibody. (*C*) Immunoblotting of membrane fraction from oocytes injected with water, rat AQP6 WT, N60G, N60A, or N60S cRNA.

for 2–3 days at 18°C in 200 milliosmolar modified Barth's solution. The oocyte swelling assay was used for osmotic water permeability measurement (19). Oocytes were transferred into modified Barth's solution diluted to 70 milliosmolar with distilled water, and the time course of volume increase was monitored at room temperature by videomicroscopy with an on-line computer (6, 16). The relative volume (V/V_0) was calculated from the area at the initial time (A_0) and after a time interval (A_t): $V/V_0 = (A_t/A_0)^{3/2}$. The coefficient of osmotic water permeability (P_f) was determined from the initial slope of the time course [$d(V/V_0)/dt$], initial oocyte volume ($V_0 = 9 \times 10^{-4}$ cm^3), initial oocyte surface area ($S = 0.045$ cm^2), and the molar volume of water ($V_w = 18$ cm^3/mol):

$$P_f = (V_0 \times d(V/V_0)/dt)/(S \times V_w \times (osm_{in} - osm_{out})).$$

Electrophysiology. Recordings were performed with isoosmotic NaCl solution (100 mM NaCl/2 mM KCl/1 mM $MgCl_2$/5 mM Hepes, pH 7.5) or isoosmotic $NaNO_3$ solution (100 mM $NaNO_3$/2 mM KCl/1 mM $MgCl_2$/5 mM Hepes, pH 7.5). The membrane potential of oocytes was controlled by using the two-microelectrode voltage-clamp technique. The command voltage was applied by a two-microelectrode voltage clamp amplifier (Axoclamp-2A, Axon Instruments, Foster City, CA) controlled by an IBM-compatible computer running PCLAMP software (Axon Instruments). Current signals were sampled at 100 μsec. In most experiments, the membrane potential was held at $V_{hold} = -50$ mV. To obtain a current–voltage relationship, the membrane potential was rapidly stepped from the holding potential to a series of values generated between +50 and −130 mV, each differing by 20 mV. The pulse duration was 100 msec, and currents from 10 runs were averaged to reduce noise. All measurements were performed at room temperature.

Oocyte Immunofluorescence and Confocal Microscopy. Oocytes were incubated in fixing solution (80 mM Pipes, pH 6.8/5 mM EGTA/1 mM $MgCl_2$/3.7% formaldehyde/0.2% Triton X-100) at room temperature for 4 h, transferred to methanol at −20°C for 24 h, equilibrated in PBS at room temperature for ≈2 h, incubated in PBS with 100 mM $NaBH_4$ at room temperature for 24 h, and bisected with blades. The oocytes were blocked by 2% BSA in PBS for 1 h at room temperature, incubated at 4°C

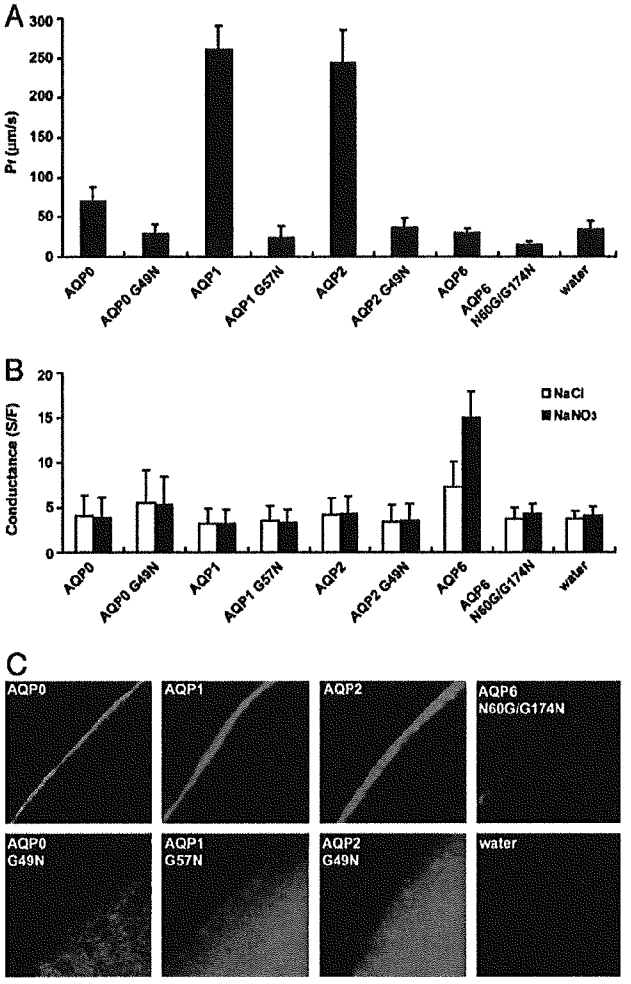

Fig. 4. The Gly to Asn mutants of AQP0, AQP1, AQP2, and AQP6 in oocytes. *X. laevis* oocytes were injected with 5 ng of AQP0, AQP1, AQP2, or the Gly to Asn mutants cRNA, or 15 ng of AQP6 N60G/G174N cRNA, and cultured for 2–3 days. (*A*) Osmotic water permeability (P_f) of AQP0 G49N, AQP1 G57N, AQP2 G49N, and AQP6 N60G/G174N. (*B*) Ion conductances of water injected, WT AQP6, or each mutant oocyte in NaCl solution (open columns) and $NaNO_3$ solution (closed columns). Conductances were calculated from slopes of I–V curves between +10 mV and −90 mV. Only the AQP6 oocyte showed conductance increase in $NaNO_3$ solution. (*C*) Confocal microscopy of oocytes injected with AQP0, AQP0 G49N, AQP1, AQP1 G57N, AQP2, AQP2 G49N, or AQP6 N60G/G174N cRNA. The oocytes were stained by the antibody against AQP0, AQP1, AQP2, or AQP6.

sequentially with rabbit anti-AQP6 antibody and Alexa Fluor 488 goat anti-rabbit IgG in blocking buffer (each for 24 h) and mounted in Fluoromount-G (Southern Biotechnology Associates). Pictures were taken with a PerkinElmer UltraView LCI confocal laser-scanning microscope.

Oocyte Membrane Extraction and Immunoblotting. Ten oocytes were homogenized together by pipetting up and down in hypotonic lysis buffer (7.5 mM sodium phosphate/1 mM EDTA, pH 7.5) including protease inhibitor mixture (Sigma). The oocyte yolk was removed by discarding the pellet after a 735 × *g* centrifugation at 4°C for 10 min. The supernatant was centrifuged again at 200,000 × *g*, 4°C, for 1 h; the membrane was harvested by collecting the pellet. The oocyte membrane was solubilized by 2% SDS, normalized by total protein amount with BCA method (Pierce), and used in 12% SDS/PAGE. The proteins were transferred to a poly(vinylidene difluoride) membrane, probed with rabbit anti-rat AQP6 antibody and horseradish peroxidase-conjugated donkey anti-rabbit IgG (Amersham Pharmacia). The enhanced chemiluminescence detection system (Amersham Pharmacia) was used to visualize the specific immunoreactive proteins by exposure to autoradiographic films.

Results

Sequence alignment of the mammalian aquaporins revealed that rat AQP6 has several unique amino acid residues: Tyr-34, Asn-60, Trp-71, and Lys-72 (Fig. 1*A*). These residues are conserved in mouse, rat, and human AQP6; all are located in TM1 and TM2 and loop B. Thr-63 and Lys-72 have been shown as key residues in AQP6 ion selectivity (8, 9). According to the atomic structural model of human AQP1, three large helical crossing angles stabilize crucial right-handed coiled-coil interactions; all have highly conserved glycine residues at the contact regions (10). For example, the fitting of ridges into grooves in TM2 and TM5 is mediated by two highly conserved glycine residues: Gly-57 and Gly-173 in human AQP1, respectively. Interestingly, we found that one of these glycine residues is replaced by an asparagine residue in rat AQP6 (Asn-60, Fig. 1*B*).

To test whether the unique asparagine residue (Asn-60) of rat AQP6 is critical for its unique anion permeability, Asn-60 was substituted by site-directed mutagenesis to Gly-60 (N60G mutant). In WT AQP6 oocytes, membrane currents exhibited substantial anion permeability. Slightly outward-rectifying currents were observed at pH 7.5 with a notable negative shift of the reversal potential immediately after replacement of the external buffer containing 100 mM NaCl with 100 mM $NaNO_3$ (Fig. 2 *A* and *B Middle*). N60G mutant oocytes and water-injected control oocytes failed to exhibit inducible currents by replacement of the external buffer containing 100 mM NaCl with 100 mM $NaNO_3$ at pH 7.5 (Fig. 2 *A* and *B Bottom* and *Top*, respectively). We knew that lack of inducible currents in N60G mutant oocytes was not due to impaired membrane trafficking of the mutant protein, because the N60G mutant was localized at the plasma membrane as well as WT AQP6 (Fig. 3*B*). Neither N60A nor N60S mutant oocytes exhibited inducible currents in 100 mM $NaNO_3$ (pH 7.5) solution, although both were expressed at the oocyte plasma membranes (Fig. 3*B*).

We examined the osmotic water permeability of N60G mutant oocytes by swelling assay. Surprisingly, N60G mutant oocytes had significantly increased osmotic water permeability (P_f = 131.62 ± 16.11 cm/s × 10^{-4}) compared with water-injected or WT AQP6 oocytes (P_f = 15.73 ± 2.50 cm per s × 10^{-4}, P_f = 12.40 ± 5.22 cm per s × 10^{-4}, respectively) (Fig. 3*A*). The Arrhenius activation energy (E_a) was lower in N60G RNA-injected oocytes (E_a < 5 kcal/mol) than in water-injected control oocytes (E_a > 10 kcal/mol) (Fig. 3*A Inset*). Increase of osmotic water permeability in the N60G mutant was due neither to increased protein expression nor to changes in protein distribution (Fig. 3 *B* and *C*). These findings demonstrate that a single amino acid substitution at Asn-60 for Gly-60 not only abolishes anion permeability but also increases water permeability. The osmotic water permeability of N60G was not inhibited or activated by $HgCl_2$ (not shown). There was no evidence of protein glycosylation of the N60G mutant, although WT AQP6 has a 30-kD glycosylated form that is cleaved by both PNGase-F and Endo-H (Fig. 3*C* and ref. 15). These findings suggest that N60G may be different from WT AQP6 in terms of its *in vivo* 3D structure or configuration.

We next tested whether the N60G/G174N mutant, exchanging the asparagine residue from position 60 to position 174, recapitulates anion permeability. Neither anion permeability nor osmotic water permeability of N60G/G174N mutant oocytes was significantly increased over that of water-injected control

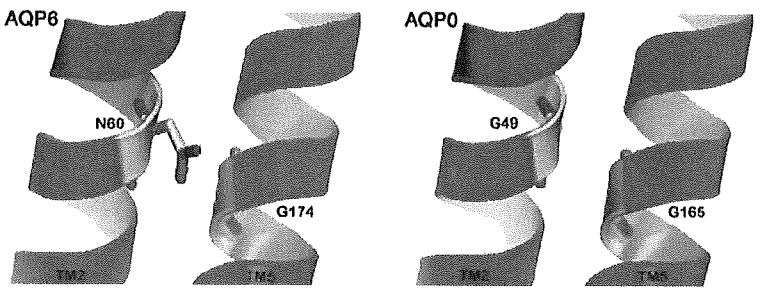

Fig. 5. Structural model highlighting the crossing point between TM2 and TM5. (*Left*) TM2 and TM5 of AQP6 structural model based on the AQP0 structure. Asn-60 and Gly-174 are highlighted. (*Right*) TM2 and TM5 in AQP0 crystal structure (18). The side chain of Asn-60 in AQP6 may affect the contact point between TM2 and TM5.

oocytes. This result may have been due to lack of expression of the N60G/G174N mutant at the plasma membrane of the oocytes (Fig. 4*C*).

To examine further the importance of the asparagine residue at the position in TM2 where it interacts with TM5, we introduced the reciprocal point mutation (Gly to Asn) in AQP0, AQP1, and AQP2. None of the reciprocal mutants revealed significant osmotic water permeability or ion permeability caused by impaired trafficking to the plasma membrane (Fig. 4).

Discussion

Recent advances in structural biology have largely explained the biophysical properties of membrane channels in terms of selectivity, conductance, and gating (20, 21). The structural model of AQP1 and molecular dynamics simulations of water transport revealed how water molecules are rapidly transported through the pore, whereas protons are excluded (22, 23). The closest homologs of AQP6 are AQP0, AQP2, and AQP5; all belong to the classical group of aquaporins selectively permeated by water (17). AQP6, however, functions as an anion channel with limited water permeability, suggesting that subtle differences in the sequence of AQP6 may lead to major differences in biophysical function (8, 9). Here we have identified a critical amino acid residue for anion permeability of AQP6, Asn-60. We have demonstrated that a single amino acid substitution at Asn-60 for Gly-60 switches the function of AQP6 from that of an anion channel to that of a water-selective channel.

Asn-60 in AQP6 corresponds to Gly-57 in AQP1, which is conserved among all other mammalian aquaporins. The atomic model of AQP1 revealed that Gly-57 is located in the middle of TM2 and interacts with Gly-174, which is also conserved among all mammalian aquaporins in the middle of TM5. The fitting of ridges into grooves in TM2 and TM5 locks the two AQP1 helical bundles together near the 4-fold axis of the tetramer (11). This implies that the structure of AQP1 is relatively rigid, and that gating of AQP1 by conformational changes is unlikely. This rigid structure might be a general feature of aquaporins. It is extremely unusual for AQP6 to have an asparagine residue at the position corresponding to Gly-57 in human AQP1. Therefore, we suspected that the residue in an important position from a structural point of view might be crucial to the unique anion permeability or gating of AQP6 (Fig. 5). We first used the human AQP1 structure because that of bovine AQP0 was not available during the study and manuscript preparation. Between human AQP1 and bovine AQP0, the glycine residues are conserved and the 3D structures at TM2 and TM5 are similar.

Our functional data support in another way the importance of glycine residues at the helical interaction sites for aquaporin structure formation. A N60G/G174N double AQP6 mutant and reciprocal glycine to asparagine mutations in AQP0, AQP1, and AQP2 all failed to traffic to the plasma membrane. These findings suggest that the interaction of TM2 and TM5 is precisely defined, and that subtle differences here lead to significant conformational changes. It may be necessary but not sufficient to have an asparagine residue at its key position for anion permeability.

We have demonstrated that Thr-63 and Lys-72 are critical residues in AQP6 ion selectivity (8, 9). Other residues, including Thr-63 and Lys-72, may allow AQP6 to have an asparagine residue at its position corresponding to the well conserved Gly-57 in hAQP1 without impairing protein folding. Also, we suspect that the pore diameter of AQP6 at its narrowest point is significantly wider than that of AQP1, because AQP6 is permeated by SCN^- and NO_3^-. The pore in AQP1 narrows to 2.8 Å, which is too narrow for these anions (24). On the other hand, the N60G mutant may have a similar pore diameter, because it is permeated by water but not by anions.

Having identified notable functional differences between WT AQP6 and the N60G mutant, we feel it is crucial to solve the structures of both WT AQP6 and the N60G mutant. We expect that a structural comparison of these mutants will give us a better understanding of how AQP6 is permeated by anions and why other aquaporins are not permeated by any ions.

We thank William Guggino and Peying Fong for critical evaluation of the manuscript and Sally Craig for editorial assistance. Support was provided by grants from the National Institutes of Health (Grants DK065098, HL48268, and EY11239), the American Heart Association, and the S&R Foundation.

1. Agre, P., King, L. S., Yasui, M., Guggino, W. B., Ottersen, O. P., Fujiyoshi, Y., Engel, A. & Nielsen, S. (2002) *J. Physiol.* **542,** 3–16.
2. Stroud, R. M., Savage, D., Miercke, L. J. W., Lee, J. K., Khademi, S. & Harries, W. (2003) *FEBS Lett.* **555,** 79–84.
3. Tsunoda, S.P., Wiesner, B., Lorenz, D., Rosenthal, W. & Pohl, P. (2004) *J. Biol. Chem.* **279,** 11364–11367.
4. Ilan, B., Tajkhorshid, E., Schulten, K. & Voth, G. A. (2004) *Proteins* **55,** 223–228.
5. Burykin, A. & Warshel, A. (2004) *FEBS Lett.* **570,** 41–46.
6. Chakrabarti, N., Roux, B. & Pomes, R. (2004) *J. Mol. Biol.* **343,** 493–510.
7. Yool, A. J., Stamer, W. D. & Regan, J. W. (1996) *Science* **273,** 1216–1218.
8. Yasui, M., Hazama, A., Kwon, T. H., Nielsen, S., Guggino, W. B. & Agre, P. (1999) *Nature* **402,** 184–187.
9. Ikeda, M., Bitz, E., Kozono, D., Guggino, W. B., Agre, P. & Yasui, M. (2002) *J. Biol. Chem.* **277,** 39873–39879.
10. Hazama, A., Kozono, D., Guggino, W. B., Agre, P. & Yasui, M. (2002) *J. Biol. Chem.* **277,** 29224–29230.
11. Murata, K., Mitsuoka, K., Hirai, T., Walz, T., Agre, P., Heymann, J. B., Engel, A. & Fujiyoshi, Y. (2000) *Nature* **407,** 599–605.
12. Sui, H., Han, B. G., Lee, J. K., Walian, P. & Jap, B. K. (2001) *Nature* **414,** 872–878.
13. Schneider, D., Liu, Y., Gerstein, M. & Engelman, D. M. (2002) *FEBS Lett.* **532,** 231–236.